scientific reports



OPEN

Sediment generation through thermal spalling during the 2021 montiferru planargia wildfire and its contribution to postfire debris flows

Costantino Pala^{1⊠}, Maria Teresa Melis¹, Laura Pioli¹, Roberto Sarro², Stefano Loddo³,⁵, Salvatore Cinus³ & Maria Teresa Brunetti⁴

Wildfires are increasing in both magnitude and frequency because of climate change and anthropogenic factors. Fire-induced changes lead to a sudden increase in the movement of sediment, making it more likely for soil particles to reach channels. As wildfire frequency increases, we are learning more about related erosional and depositional phenomena, including thermal spalling. Thermal spalling happens when rocks crack due to sudden temperature spikes. Dramatic temperature changes cause pore pressure increases and mineral dilation resulting in fracturing and spalling from rock exposures and fragmentation of existing debris. In this study, we observed a rocky Mediterranean area with a dense oak forest and shrubberies that was partially burnt during the 2021 Montiferru-Planargia wildfire. Before the fire, rockfalls had deposited debris under the forest canopy. Thermal spalling eroded exposed rocks and boulders, generating new deposits. This loose sediment increases debris flow, especially during rainstorms after fires. In the burnt scar, 33 debris flows occurred in the two years postfire showing clear impacts of thermal spalling whose signs are observed in the clasts transported by flows. Our results indicate that thermal spalling is a significant sediment source for post-fire debris flows and should be integrated into hazard modelling.

Keywords Wildfire, Thermal spalling, Sediment connectivity, Remote sensing, Debris flow, Susceptibility

The frequency and impact of wildfires are increasing worldwide because of climate changes inducing warmer temperatures and droughts in many areas. Million of km² are burnt yearly in our planet accounting for millions of livestocks and economic losses.

In fact, wildfires change the physical and chemical properties of soils and rocks due to heating and interaction with vapours produced by burning vegetation¹. Moreover, during a wildfire, steep temperature gradients between the soil surface and the dry mineral soil can cause hydrophobic compounds from burnt vegetation to move into the soil, forming water-repellent layers^{1,2}. These layers reduce water infiltration and increases surface runoff during post-fire rainstorms^{3–6}. Additionally, the fire disrupts soil structure and colloidal compounds, further increasing erosion. The removal of vegetation by wildfires also enhances sediment connectivity, leading to higher sediment yield from debris flows^{7,8}. Debris flow is defined as a rapid mass movement of silty water, broken rocks, earth and other inorganic material⁹. Mass movements can also begin following progressive sediment entrainment or by infiltration-dominated processes¹⁰.

Wildfires typically occur during droughts and are associated with temperatures over 800 °C¹¹. Wildfires only heat the outer layers of rocks for a short time (minutes), causing intense thermal stress between the hot outer shell and the cold inner core. High temperatures induce different reactions in rocks, such as volume changes, increased pore pressure, and crack formation. Moreover, surface rocks are often preserving humidity within

¹Department of Chemical and Geological Sciences, Cagliari State University (UNICA), Cittadella Universitaria di Monserrato, Monserrato 09042, CA, Italy. ²Department of Geohazards and Climate Change, Geological and Mining Institute of Spain (IGME-CSIC), Ríos Rosas 23, Madrid 28003, Spain. ³Autonomous Region of Sardinia − General Directorate of Civil Protection, Via Vittorio Veneto 23, Cagliari 09123, CA, Italy. ⁴Research Institute for the Hydrogeologic Protection − National Research Council (CNR-IRPI), Via Madonna Alta 126, Perugia 06128, Italy. ⁵Stefano Loddo is deceased. [△]email: costantino.pala@unica.it

pores and fractures. When fluids are heated, they can vaporise, increasing pore pressure. Rock-forming minerals react differently to heating. These changes are due to rearrangements in the crystal structure and variations in water content which can result in an increase or decrease of density. Common minerals like quartz, feldspathoids, and alkali-feldspar can undergo phase transitions during wildfires. For example:

- Quartz a quartz b transitions at 574.3°C^{12,13}.
- K feldspar phase transitions around 500°C¹⁴.
- Sodalite to nepheline transition between 800 and 900°C¹⁵.

Existing cracks in rock masses influence how heat flows through them. Cracks that are perpendicular to the heat flow reduce heat transfer, while parallel cracks make it more efficient¹⁶. Rock masses have various cracks from different geological events, and the overall effect on heat transfer can be described by the density of these cracks¹⁷. Differential volume changes and pore pressure gradients induce further rock fracturing and spalling^{18–21}. Spalling is a primary effect of thermal fracturing^{22–25}. This process is well studied in fires within road tunnel or ducts^{26,27}, but poorly in wildfires, with limited field data available^{18–21}.

Very high and very low thermal conductivity rocks are unlikely to experience thermal spalling because they either conduct heat well or are well-insulated, making it improbable for a significant temperature difference to form between the surface and the inner layers during a fire ²⁸.

Despite the existing research on the mechanics of fire-induced spalling, little is known about the geomorphological effects of spalled material on postfire processes. We present data on the impact of the Montiferru-Planargia 2021 wildfire (Fig. 1), as a valuable case study for understanding the impact of wildfires on sediment production, runoff, and yield in Mediterranean mountain regions. This region has been frequently affected by wildfires over the past 40 years and offers an ideal natural laboratory due to its accessibility and availability of pre-wildfire data. The area features thin, highly erodible soil on steep slopes stabilized by vegetation^{29,30}. Before the fire, erosion was mainly due to rockfalls and slides.

2021 Montiferru fire dynamics

On July 24–25, 2021, a wildfire (Figs. 1 and 2a) began in Sardinia (Italy) around 5:00 pm near Santu Lussurgiu village and, within twelve hours, spread to Porto Alabe, a coastal village 20 km away. The event was classified as a megafire, with 40-meter-high flames creating pyrocumulonimbus clouds and sparking new fires kilometers away from the main blaze³¹.

The wildfire had two main phases:

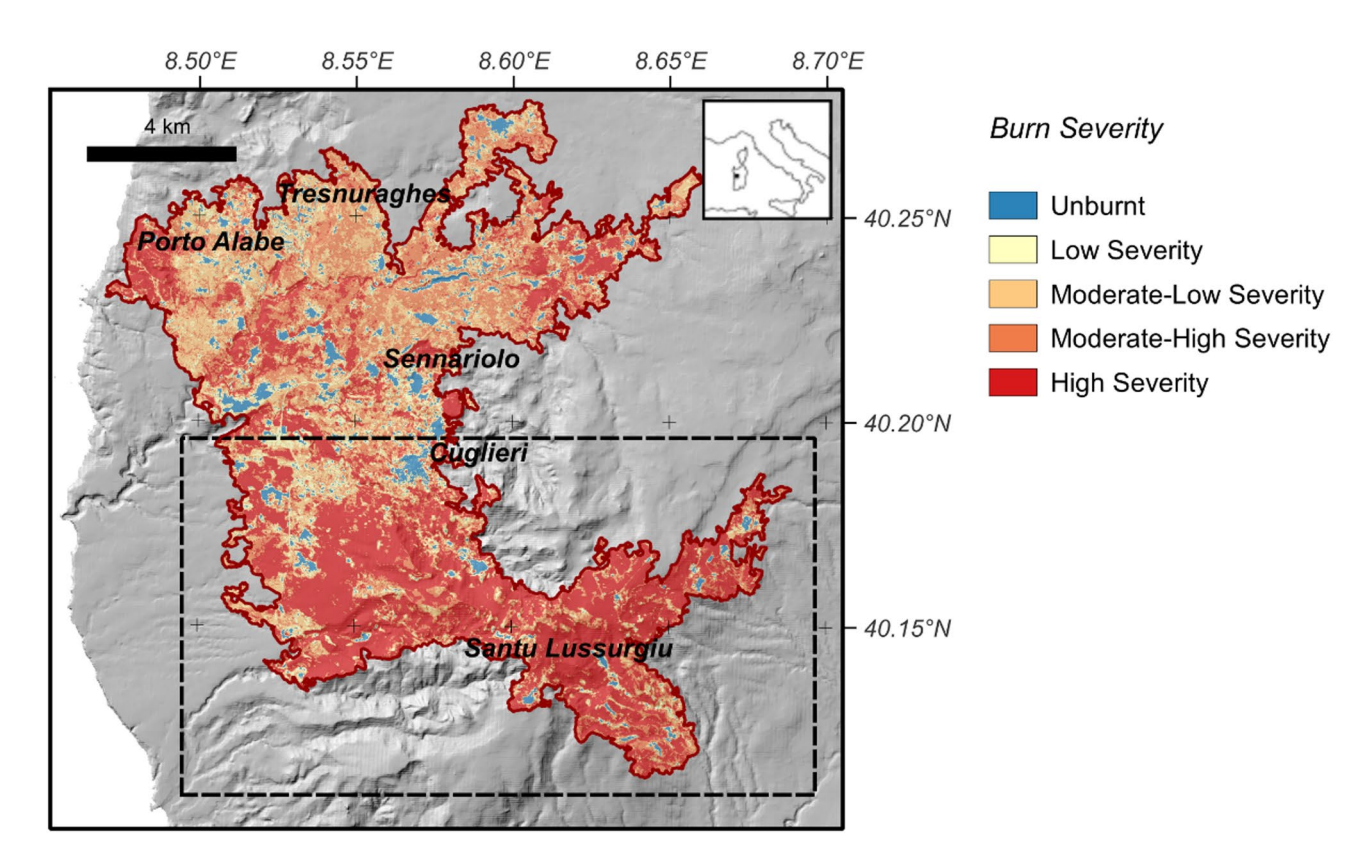


Fig. 1. Map of the total burnt area and its surroundings. The map shows data for elevation and burn severity classes. The black dashed rectangle highlights the study area. Image generated with QGIS version 3.34.11-Prizren (https://qgis.org) and Inkscape 1.4 86a8ad7, 2024-10-11 (https://inkscape.org).

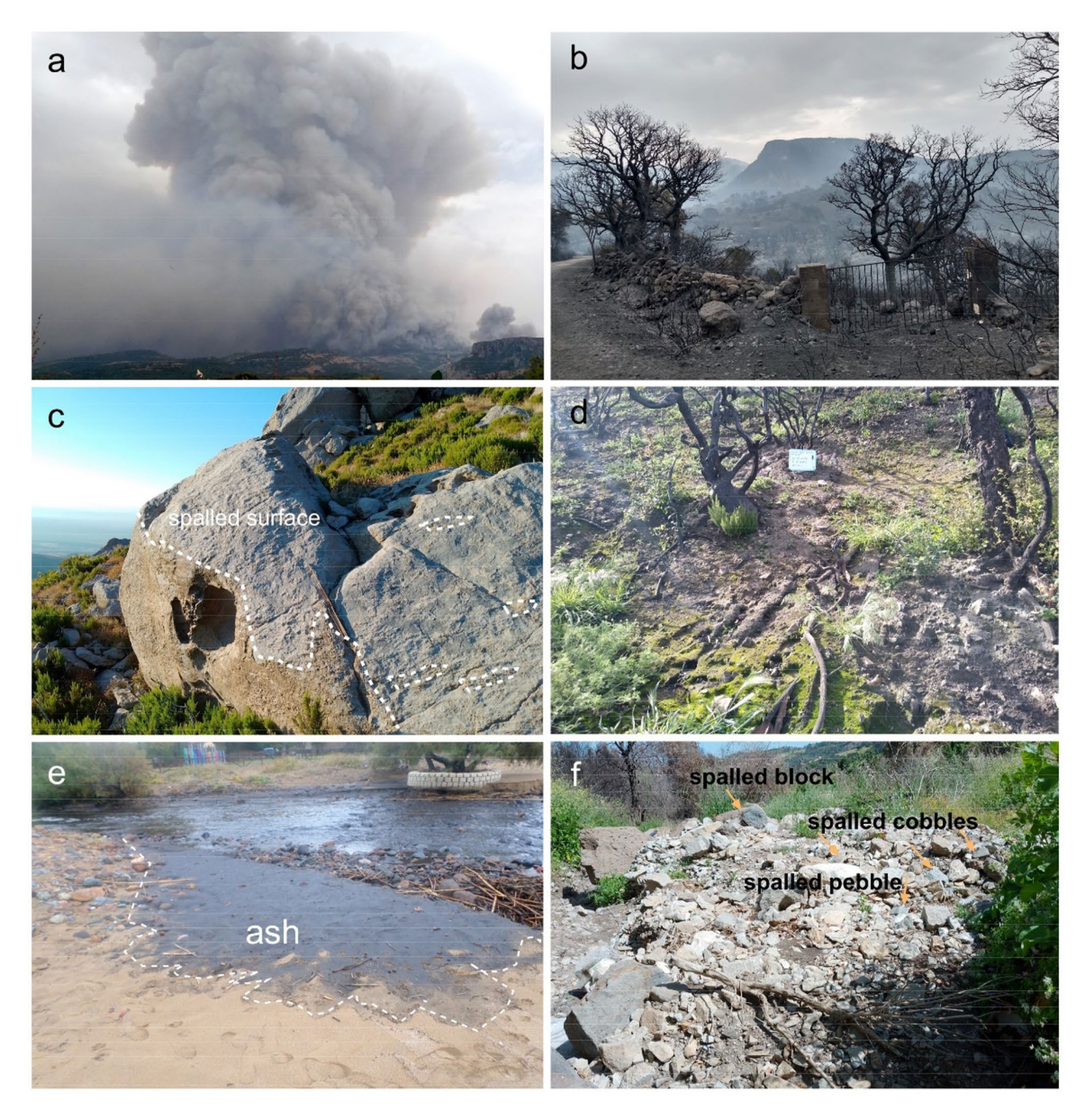


Fig. 2. Table with photographs of wildfire, synfire and postfire landforms. (a) First stages of the fire near Santu Lussurgiu at 6:00 pm on 24th July 2021. (b) Burnt forest few hours after the fire and evidence of spalling on building blocks made of Santa Caterina di Pittinuri marls. (c) Tephrite-phonolite boulders related to pre-fire rockfall activity with clear signs of thermal spalling. (d) Rill-interrill erosion on soils formed on Pliocene debris avalanche deposit. (e) overbank deposits made by fire ashes and organic debris close to the sea. (f) postfire debris flow deposit with clastic material showing clear evidence of thermal spalling and syn-flow fracturing. Image generated with Paint.NET version 5.1.7 stable 5.107.9212.41708 (https://www.getpaint.net) and Inkscape 1.4 86a8ad7, 2024-10-11 (https://inkscape.org).

- Initial ignition and spread, lasting about 8 h, with crown burning and strong winds, causing damage to private
 and public buildings.
- Further spread to the northwest and northeast, with small reignitions in the previously burnt area. Ground fires continued in the following 7 days burning tree roots and causing random reignitions.

The burnt forest consisted of Mediterranean vegetation, including species such as holm oak (Quercus Ilex), cork oak (Quercus Suber), stone pine (Pinus pinea), Aleppo pine (Pinus halepensis), maritime pine (Pinus pinaster),

Canary Island pine (Pinus caneriensis), and shrubs like strawberry tree (Adutus unedo), broom heather (Erica scoparia), mock privet (Phillerea angustifolia), thorny broom (Callicotome spinosa), rockrose (Cistus sp.), myrtle (Mirtus communis), and juniper (Juniperus sp.)³² (2b).

The wildfire damaged civil structures in the countryside and in the urban areas of Cùglieri, Sennariolo and Tresnuraghes and was declared extinguished on July 30. About 1450 people were evacuated from 24 to 30 July. This area has experienced previous forest fires in 1983 and 1994, but post-fire erosion processes were not documented. The Montiferru region has a hot-summer Mediterranean climate with warm, dry summers and a rainy period from November to March³³. Snowstorms and hailstorms can also occur between December and February. In total expenses for emergency management accounted for more than 1.8 million euros; losses associated with damage to infrastructures and economic activity accounted for about 5 million euros. About 1000 livestock losses were reported, and 400 apiaries (about 36 million bees) were destroyed³⁴.

Geology of the area

The landscape of the study area is largely inherited from the volcanic activity of the Montiferru Volcanic Complex and, in particular, from the most recent volcanic phase, which occurred from 3.9 to 1.6 Ma ago^{35,36}. This volcanism is emplaced on Miocene caldera deposits, lavas, marls and limestones³⁷. Rocky hills and peaks are composed by tephrite, phonolite and trachyte lava domes and flows (hereafter, tephrite-phonolite lavas), consisting of Sanidine \pm plite \pm Analcime \pm Nepheline \pm Nosean \pm Sodalite \pm Biotite \pm Pyroxene \pm Plagioclase \pm Phlogopite \pm Amphibole³⁸. The lavas are well exposed in the summits, whereas the mid-bottom slope sectors are occupied by partly eroded autobreccia, covered by colluvium and < 1 m thick soils. Gentle slopes are formed by trachybasalt lava flows containing Pl + Cpx \pm Ol³⁸. In this area these flows are usually a few meters thick and mantle older lavas and breccia deposits. Pliocene-age debris avalanche and flow deposits are intercalated in the lava dome activity and covered by the later trachybasalt flows³⁷.

Most of the area is covered by colluvial deposits, soils, rockfall deposits such as debris cones, scree slopes, and scattered boulders. Rockfalls are linked to dome erosion and flow borders. Additional slope failures have occurred on Pliocene debris avalanches and colluvial deposits. Erosion terraces formed in the valley bottoms on alluvial deposits. Pre-wildfire soils were classified as Lithic Udipsamment, Lithic Distrudept and Humic Lythic Dystroxerept³⁹. Soils exposed in the burnt area occupied by Miocene pyroclastic density current (PDC) deposits and debris avalanche deposits are described as Andic Dystrudepts and characterized by a high thixotropy⁴⁰.

Results

Fire mapping

A burn severity map was compiled based on multispectral ESA Sentinel-2 L2A data⁴¹ to quantify the fire impact on vegetation (Fig. 1). The burnt area has a perimeter of 65.91 km and covers 131.64 km². Within this area, 6.60 km² remained unburnt. Of the burnt area, 63.1% was classified moderate-high to high severity, indicating dense vegetation in the southern part of the study area, which was originally covered by forest and shrubberies.

The fire left a layer of fine ash from burnt vegetation, which settled on the ground and was later remobilised by wind, forming deposits up to 60 cm thick in channels (Fig. 2b). Logs, branches, and burnt leaves were scattered on the surface, but in most cases, except pine trees, there was no root fire and plants began producing new shoots within a month.

The detail analyses of the fire impact will focus on the southern portion of the scar, where most of the high severity areas are located (Figs. 1 and 2).

Pre-fire sediment production and Geomorphological processes

The assessment of geomorphological processes active in the area before the fire was based on field surveys and aerial and satellite data from the past sixty years for photo-geological analysis. Rock exposures, identified from satellite images identifying 47 points, mostly rock peaks, counted as areas with zero soil or colluvium thickness. Soil and colluvium deposits thicknesses maps, calibrated in 631 points are shown in Fig. 3a, b. Measurements were performed on August 2022 but the prefire soil surface was still observable in the areas were rill-interrill and earth pyramid erosion occurred, so we estimated an uncertainty of 7 cm (minimum erosion observed is 3 cm and maximum 13 cm).

Moreover, we compared these thicknesses with soil depth data collected in the same area on 2002⁴⁰. This comparison confirms the soil thickness distribution in this area. Soils are not uniformly distributed in the study area; they reach maximum thickness of 230 cm and are thickest in the western sector; the eastern sector lacks soil cover. Colluvium thickness map revealed similar distribution patterns and confirming low levels of loose sediments before the wildfire (Fig. 3a, b). The deepest deposits were found in the western area, near the edge of a dome complex. Soils were thickest on Plio-Pleistocene alluvial fan, debris avalanche, and PDC deposits. Trachybasalt and tephrite-phonolite lavas usually had shallow soil cover, rarely exceeding 130 cm (Fig. 3c, d). There are no colluvial deposits on alluvial fans, poorly developed on trachybasalt lava flows and pyroclastic density current deposits but well developed on Pliocene debris avalanche deposits, and tephrite-phonolite lavas (Fig. 3c, d). Steep slopes were dominated by rock exposures, debris and large boulders from rockfalls and scarce silt and soil. The main active sedimentary processes were rockfall, landslides, and anthropic erosion. The rockfall debris formed scree deposits, debris cones, or were limited to scattered boulders (Figs. 2c and 4a, Figure S3). Prefire afforestation terraces were also mapped owing to their well-known property of blocking overland flow erosion⁴². The same effect of terracing has been observed on slopes settled on stacked rims of eroded trachybasalt lava flows (Figure S3).

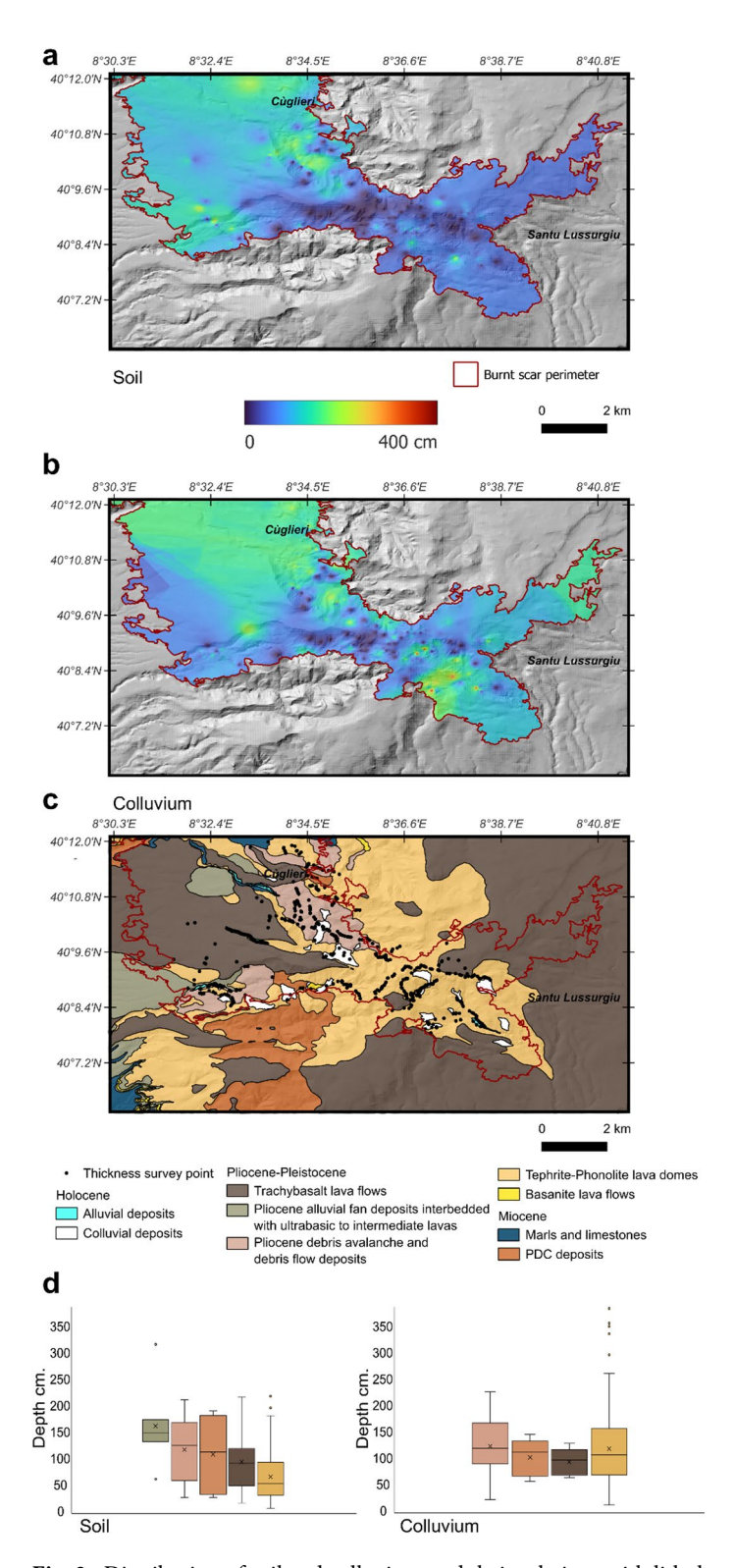


Fig. 3. Distribution of soil and colluvium and their relations with lithology. (a) Soil is mainly distributed across the periphery of the volcanic complex. (b) colluvium is thicker in the eastern sector of the Complex and in the periphery. (c) Most of the study area is settled on tephrite-phonolite lavas and debris avalanche deposits. (d) thickness distribution of soil and colluvium and their relations with the rock type. Soil has narrow distributions in relation to colluvium deposits and has an average thickness of 50 cm on tephrite-phonolite lavas. The box plots show the largest and smallest values, 25% and 75% quartiles, median (straight line), mean (as a cross) and the outliers. Image generated with QGIS version 3.34.11-Prizren (https://qgis.org), Microsoft Excel for Microsoft 365 MSO (Version 2503 Build 16.0.18623.20208) 64 bit (https://www.microsoft.com/en-us/microsoft-365/download-office) and Inkscape 1.4 86a8ad7, 2024-10-11 (https://inkscape.org).

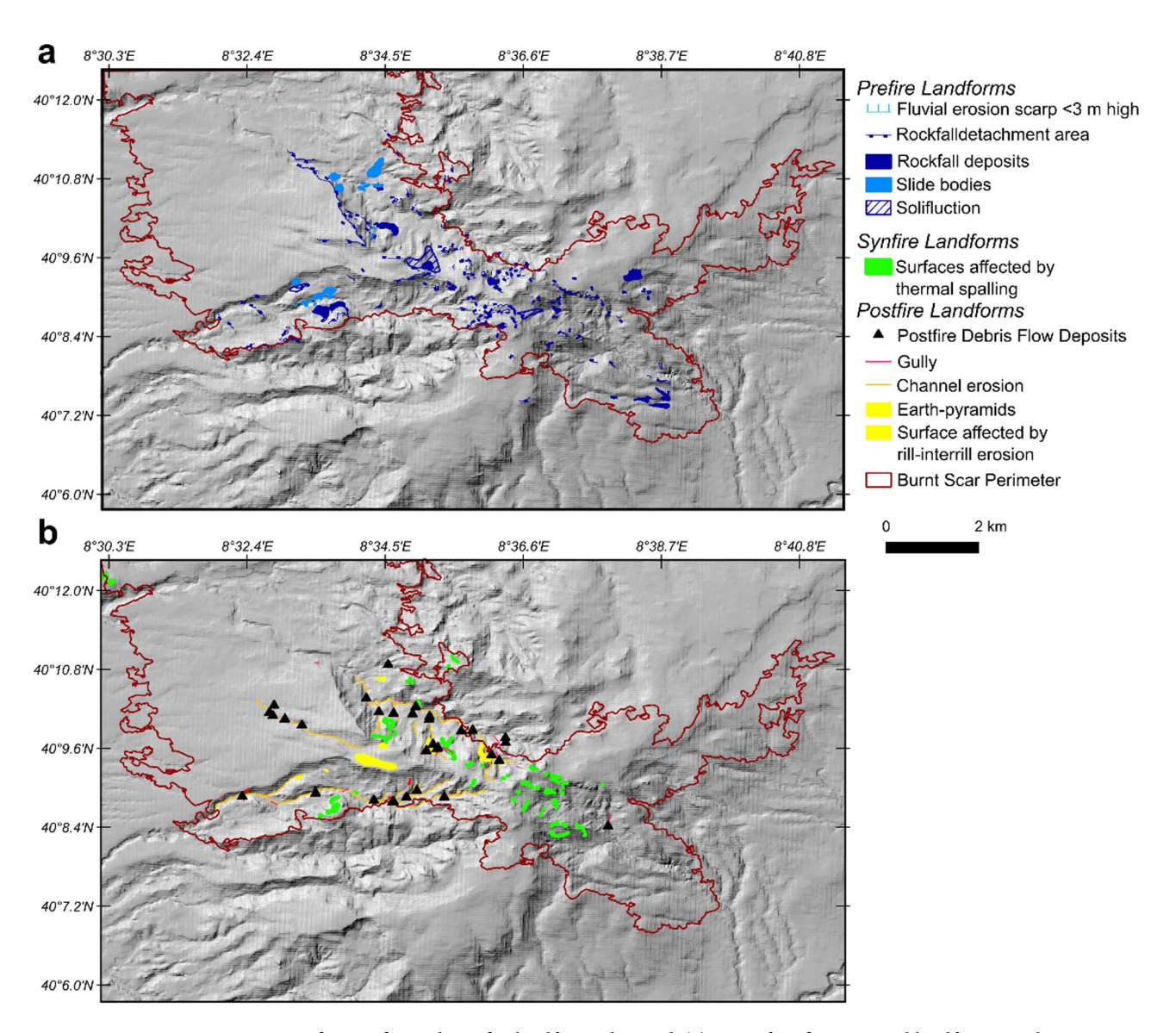


Fig. 4. Prefire, synfire and postfire landforms detected. (a) Map of prefire erosional landforms: rock detachment areas and debris cone. (b) Map of spalling areas and erosion (channel, rill, gullies) associated with debris flow (triangles) Image generated with QGIS version 3.34.11-Prizren (https://qgis.org) and Inkscape 1.4 86a8ad7, 2024-10-11 (https://inkscape.org).

Fire dynamics and impact

Thermal spalling affected exposed rocks during the fire and was observed in 69 exposures, mostly on tephrite-phonolite lava, subordinately on hydrothermally altered PDC deposits, and in scattered areas in trachybasalt lava just after the wildfire (Figs. 2c and 5b). Erosion at rock exposures was marked by fresh scars and spalls around them (Fig. 2c). It was also observed in boulders in streams, showing significant fragmentation and detachment of material. Spalling occurred equally in areas if high and moderate high burn severity; was sparse in areas of moderate low and low severity (Fig. 5a). Surface spalling occurred when thin outer layers of rock exposures flaked off and spalling fragmentation occurred mostly on loose boulders when the block broke apart due to extreme and uneven thermal stresses. The fragments ranged from 3 mm to 13 cm in thickness regardless of the lithology. The rock surface affected by thermal spalling was measured in 69 exposures and varied between 0.07% and 74.57%, with a median value of 20.3 +- 19%. Grain size distribution for spalled material is estimated on a deposit placed under a spalled cliff. Spalling occurred not only at the expenses of the cliff but also on debris formed before the fire. Pebbles constitute the 74.8% of the deposit followed by cobbles (23.2%) and gravels (2%). Rock erosion by the Montiferru fire is linked with shrubberies and forests (Fig. 5b). Data suggest that the extent of spalling is larger in fragmented rocks (i.e. debris avalanche deposits) with respect to more massive lithofacies (Fig. 5c).

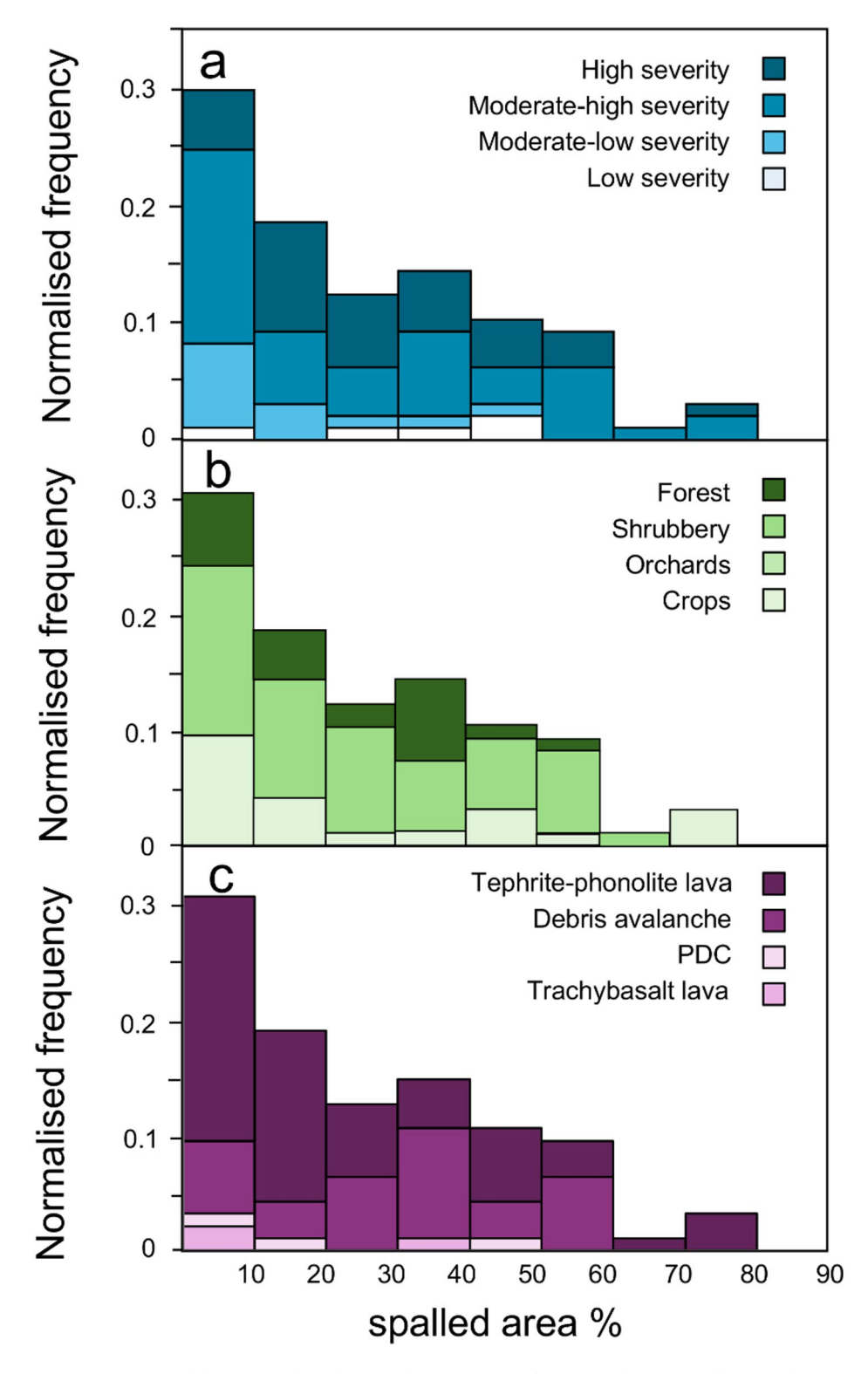


Fig. 5. Normalised frequency distribution of parameters influencing thermal spalling. (a) burn severity, (b) land cover (c) lithology. Higher erosion is associated with moderate-high to high severity, shrubberies, debris avalanche and tephrite-phonolite lavas. Image generated with Microsoft Excel for Microsoft 365 MSO (Version 2503 Build 16.0.18623.20208) 64 bit (https://www.microsoft.com/en-us/microsoft-365/download-office) and Inkscape 1.4 86a8ad7, 2024-10-11 (https://inkscape.org).

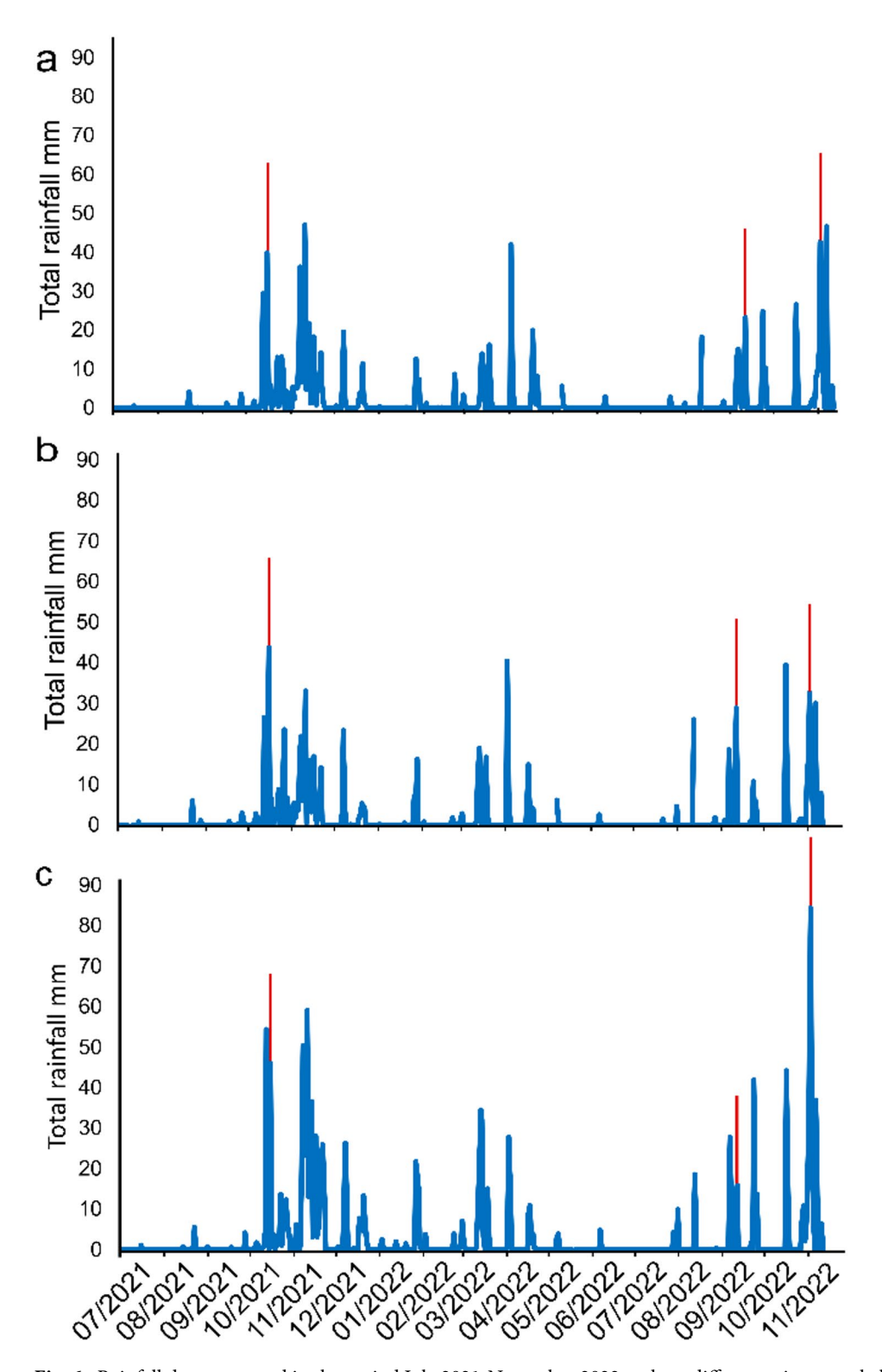


Fig. 6. Rainfall data measured in the period July 2021-November 2022 at three different raingauges belonging to the ARPAS network. (a) Cuglieri RU weather station. (b) Cuglieri C.ra Tega weather station. (c) Santu Lussurgiu RU weather station. The red line indicates the timing of the observed postfire debris flow events. Image generated with Microsoft Excel for Microsoft 365 MSO (Version 2503 Build 16.0.18623.20208) 64 bit (https://www.microsoft.com/en-us/microsoft-365/download-office) and Inkscape 1.4 86a8ad7, 2024-10-11 (https://inkscape.org).

Post wildfire debris flow triggering rainstorms

After the wildfire 33 post wildfire debris flows associated to three rainstorm events were detected in the area. The postfire rainstorms happened on 3 November 2021, 30 September 2022 and 21 November 2022. The 3 November 2021 rainstorm was associated with most of the post wildfire debris observed for a total of 24 deposits. Observed cumulates at Cuglieri RU (Fig. 7a), Cuglieri C.Ra Tega (Fig. 7b) and Santu Lussurgiu RU (Fig. 7c) ARPAS raingauges (hereafter reported in this order without referring to the station) are of 39.8 mm, 43.8 mm and 46.2 mm respectively. The 30 September 2022 event is associated with 3 deposits and cumulates of 23.2 mm, 28.8 mm and 16.0 mm. The 21 November 2022 event is associated with 7 postfire debris flow deposits and cumulates of 42.6 mm, 32.6 mm and 84.4 mm.

Post-fire erosion and transport

The area was monitored for two years after the event. Between 30 July 2021, when the wildfire was completely extinguished, and 3 November 2021, when the first postfire rainstorm occurred, the ash layer was remobilised by windstorms, and no significant transport of larger particles occurred. From 3 November 2021 to 21 November 2022, 33 post-wildfire debris flows, associated with 3 rainstorms, were observed in 21 sub-basins (Supplemental material Table S5). Burnt slopes were mainly affected by overland flow: erosion from sheet-wash, rill-interrill, and rain-splash remobilised ash, soil particles, burnt vegetation, spalls and prefire rockfall deposits. Debris masses clogged channels forming temporary dams. The dams created small and isolated basins that progressively got filled with material until breach, triggering further debris flows and channel bypass, plunge pool excavation and bank failures (Fig. 4b).

New gullies and rills formed in the areas which were not previously affected by overland flow processes. The dam-and-breach mechanism was also seen in smaller landforms along the slopes. Rills were blocked by individual pebbles, leaves, sprigs, and gravels. Gullies were blocked by bank failures and heaps of cobbles, branches, and leaves. In streams, damming triggered lateral flows, erosion, and morphology and changes. Distal deposits consisted mostly in thin (> 1 cm) layers settled from hyper concentrated flow in coastal areas (Fig. 2e).

Post-fire debris flow deposits included angular phonolite lava cobbles and boulders, in addition with rounded lava cobbles, marked by surface alteration and patina. Some large boulders exhibit complex surfaces marked by fresh, unaltered scar cutting rounded varnished surfaces, suggesting recent fragmentation either by spalling or syn-flow fragmentation. We quantified spall percentages over six postfire debris flow deposits, finding that spall percentages are comprised between 1.3% and 36.6%. Some boulders showed geometries in all similar to spalling observed on rock exposures (Fig. 2c). Although very variable, it can be estimated based on the picture taken at

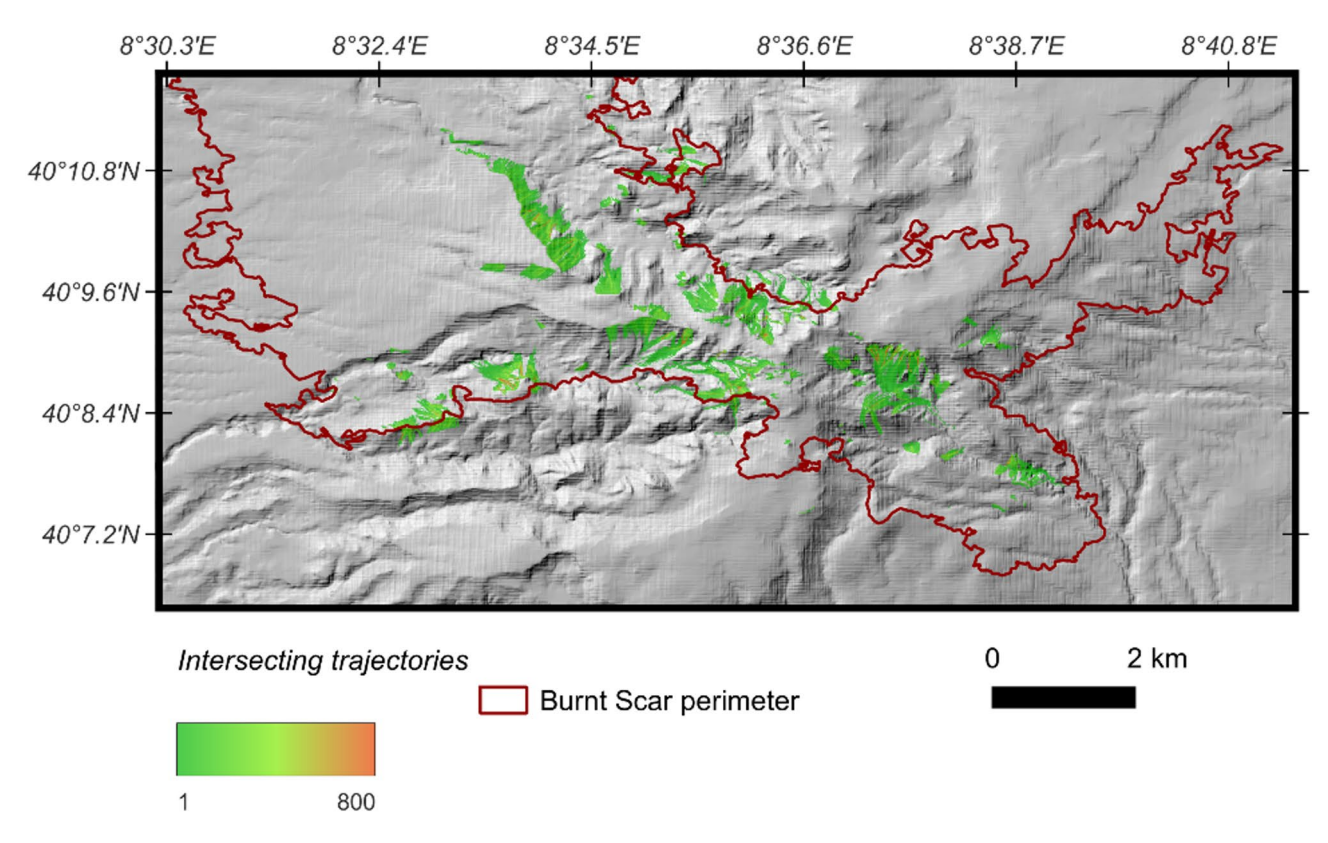


Fig. 7. Pre fire rockfall trajectories runout calculated using the STONE model. Colored area mark zones of high concentration of trajectories and indicate various detachment area classes as in legend. Image generated with QGIS version 3.34.11-Prizren (https://qgis.org) and Inkscape 1.4 86a8ad7, 2024-10-11 (https://inkscape.org).

different locations that recently spalled, angular cobbles ranged from 10 to 30% of the total amount of cobbles in the deposit.

In the second rainy season (October–November 2022), debris flows occurred in only eight sub-basins, likely because of because of vegetation recovery and/or reduced sediment supply. Debris consisted of logs, branches, leaves, soil particles and rock fragments. By the third winter after the fire (2023), the area was mostly covered with herbaceous vegetation, forbs and new shrubs, and precipitations triggered only widespread flooding.

Rockfall modelling

Rockfall is a process capable to deliver sediment downslope and to the channel area. Rockfall modelling allow to indirectly assess rockfall deposit distribution in the area.

165 rockfall detachment areas were identified and used in the model. These areas are mainly located at erosional escarpments and include both exposures previously affected by gravitational instabilities and exposures which were affected by thermal spalling during the fire. (Fig. 7). The detachment areas were categorized into three classes based on the maximum expected runout of boulders (trajectories lengths).

- Class 1, low hazard: short paths (57.1% of detachment areas).
- Class 2, moderate hazard: medium paths (19.9% of detachment areas).
- Class 3, high hazard: long paths (22.9% of detachment areas).

Most paths fell into the channels, leading to most rockfall deposits in the valley bottom. The channels mainly contained paths from Class 2 and Class 3 sources, which make up 42.8% of the detachment areas.

Most of the detachment areas in classes 2 and 3 are associated with lava domes (Table 2 of supplemental material and Fig. 8). These areas can provide sediment to the channels, potentially causing damming.

The simulations showed that 61% of the actual boulders were into areas in which rockfall processes were modelled by STONE. The remaining 39% of boulders, which were located in areas which were not included in the rockfall STONE simulations, were likely associated with less apparent or small detachment areas, volcanic autobreccia, Pliocene debris avalanche, or secondary displacements.

Distribution of parameters proposed for hazard assessment

Investigated parameters proposed for debris flow assessment show clearly different distribution across the two groups of burnt watersheds. The group exposed in the Fig. 8a (hereafter Group A) is representing watersheds were postfire debris flow activity is observed, therefore, the 8b (hereafter Group B) represents watersheds where debris flow activity is not observed after the fire.

Average IC, Average and Maximum slope have a higher mean respecting the Group B and have a narrower distribution. These parameters are chosen to represent quickly postfire erosion and debris flow hazard, since are fast and cheap to compute. The map for Sediment Connectivity Index is available in the Figure S1.

Average Burn Severity has narrower distribution in the group A and also the higher values. On the other hand, lower average severity values are observed in the group B.

In this work we investigated the potential for soil, colluvium, rockfall deposits and thermal spalling to be sources for debris flow triggering. To represent rockfall deposits we choose to use the maximum number of observed intersecting trajectories since it can be a good representation of sources related to this process. Moreover, highest rockfall trajectory intersection occurs in the channel area (Figure S3). As clearly observable in Fig. 7 the highest number of intersecting trajectories is observed in channels, therefore, high rocky debris concentrations can be expected there.

The other sources of sediment for debris flow in the study area are represented by soil and colluvium depth and thermal spalling percentages. To investigate the role of soil and colluvium as sediment sources we choose to calculate the majority for each watershed whereas thermal spalling is well represented by percentages and does not need further processing. By comparing the graphs in Fig. 8 soil and colluvium mean, median, 25 and 75 percentiles are significantly lower in the group were postfire debris flow are observed. On the other hand, thermal spalling median, mean, 25 and 75 percentiles are significantly higher.

Terracing is investigated for its known potential to mitigate erosion. Many watersheds in the study area have terraced area due to prefire afforestations (Figure S3). Mean and median are similar between the two groups, but wider terraced areas are observed in the Group B suggesting that in the case of the 2021 Montiferru Wildfire Burnt Scar terracing was effective at preventing debris flow and overland flow.

Discussion

The 2021 Montiferru-Planargia wildfire significantly impacted sediment formation, yield and transport in the area. Because of its volcanic origin, the geomorphology and soil cover distribution of the area are not homogenous. Before the wildfire, the region experienced rockfalls, solifluction and slides mainly due to human activities. In the study area, which was affected by the highest severity wildfire, the soil cover is thin and sparse in the east sector, and more developed in the west. Rock exposures (lava domes and flows) are in the SE area (Fig. 3).

Wildfire impact on sediment production and transport can be summarized as below.

During the fire:

- A widespread ash cover formed over the formerly vegetated areas.
- Sediment in the form of flakes and pebbles were formed due to thermal spalling in rock exposure and rockfall deposits.

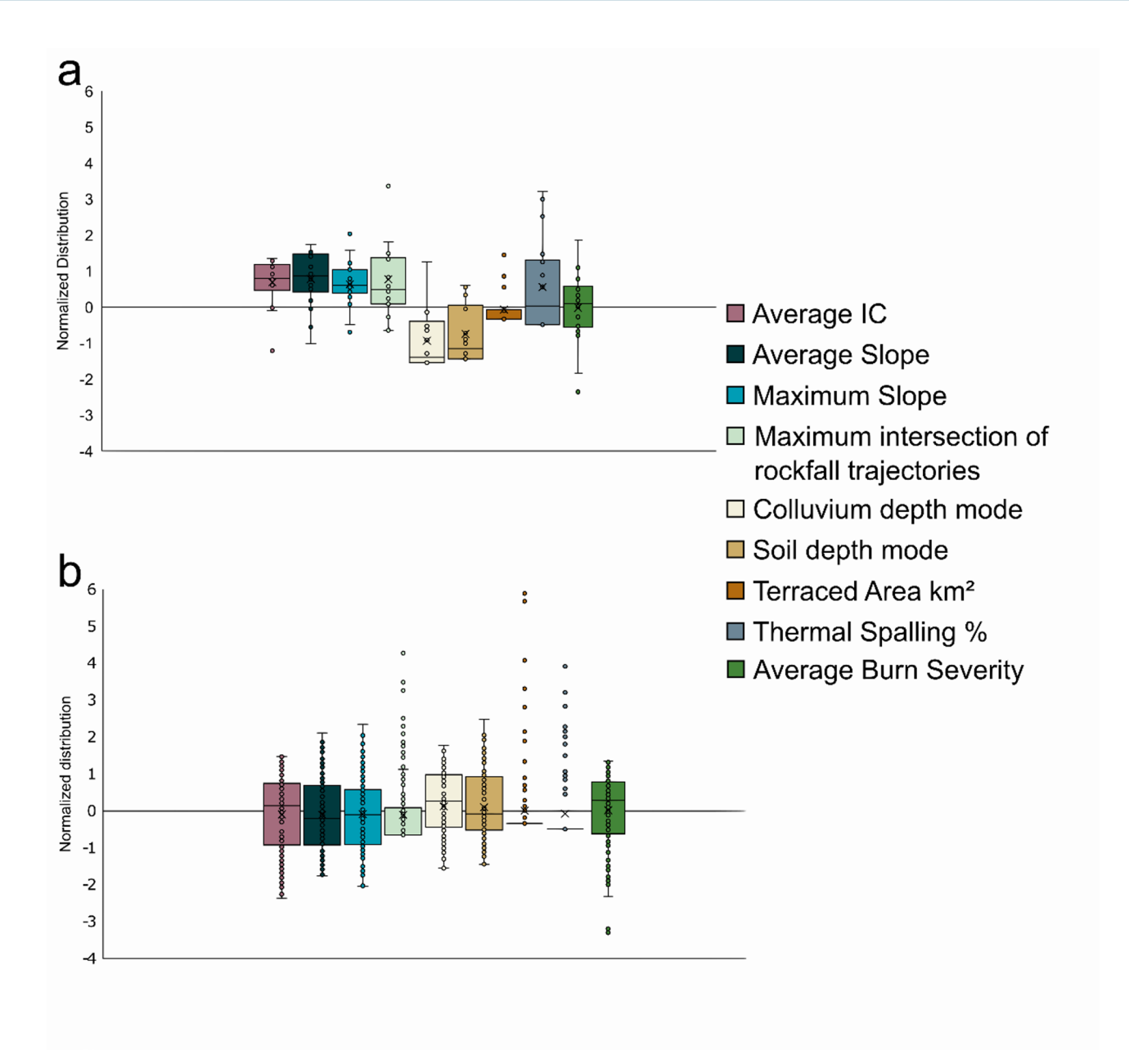


Fig. 8. Z-normalized distribution of investigated parameters across burnt watersheds. (a) Burnt watersheds which responded with debris flow activity. (b) Burnt watersheds which did not experienced debris flow. Image generated with Microsoft Excel for Microsoft 365 MSO (Version 2503 Build 16.0.18623.20208) 64 bit (https://www.microsoft.com/en-us/microsoft-365/download-office) and Inkscape 1.4 86a8ad7, 2024-10-11 (https://inkscape.org).

- After the first rainstorm on the area, four months after the fire:
- Ash and organic debris were transported to the sea coast as hyperconcentrated flows and debris flows.
- In the first 18 months after the fire:
- New erosion of soil cover and remobilisation of old rockfall deposits occurred during and after rainstorm events.
- Coarser sediments (boulders, cobbles, pebbles, gravel) were transported as debris flows.
- After 18 months after the fire:
- Vegetation recovered over most of the area (shrubberies replaced forests, forbs and herbaceous covers were restored) and erosional phenomena returned to prefire levels, likely due to increased vegetation cover in detachment areas and consequent sediment disconnection⁴³.

The wildfire impact on sediment production is a complex function of different parameters such as burn severity, soil cover distribution and spalling phenomena^{19,44,45}. Postfire erosion of soil cover is enhanced by increased runoff and gullies and rills develop in areas previously unaffected by erosion^{46–48}. These phenomena occur

typically in areas with hot summer climate and a single rainy season such as midlatitude coastal areas. As could be expected, in the study area they were limited to the zones where soil cover exceeded 15 cm (Figure S2).

Sediment is also produced during the fire; in the Montiferru fire spalling phenomena were ubiquitous on rock exposures in areas with moderate-high to high burn severity. Thermal spalling a well-known but poorly quantified phenomenon^{18,19,44,49}; we documented up to 75% of fragmentation of exposed rock surfaces. As previously suggested⁴⁴spalling was more effective in areas where burning vegetation exposed loose boulders and rock cliffs to high temperatures. Montiferru Sodium-phonolites, tephrites and trachytes are particularly susceptible to thermal fracturing because of their mineral content (sanidine, nepheline and olivine phenocrysts): feldspathoid and olivine are subjected to up to 3 times while alkali-feldspar to 0.5 volume increases during heating from 20 to 400 °C⁵⁰but spalling was more effective on fragmented lithofacies such as phonolites within the debris avalanche deposits, demonstrating that spalling is also enhanced by any internal fracture system.

By comparing the distribution of investigated values we understand that IC, Average and Maximum Slope, Rockfall Intersecting trajectories, Thermal Spalling percentages and terraced areas can be effective at predicting postfire hazard. Burn Severity seems to be a valuable hazard indicator but its role in this area is buffered by its wide areal distribution.

Since slope is a fundamental parameter in IC calculation and, given their similar distribution, we can propose to consider only IC has input factor because it allows to consider also the effects of other parameters, including Burn Severity, which is demonstrated to be well correlated with this parameter.

Rockfall intersecting trajectories is an interesting parameter not only because has a positive correlation with debris flow observation in this area but also for the well-known link between wildfire and rockfalls^{23,24}. By comparing the Figure S3 it is clear that many of the sources for rockfall activity identified in this study were also eroded during the wildfire. We can hypothesize that the sources not eroded during the 2021 Wildfire can be eroded in past fires (e.g.: associated with a different land cover class).

Rockfall simulations are also interesting owing to the higher probability of synfire erosion on boulders ^{18,19,44}. Since trajectories represent clearly deposition areas the outputs of STONE can be effective to identify synfire rocky debris sources in both channel and slope area being able to represent also debris remaining by past fire activity which not resulted in debris flow, maybe for lacking triggering conditions.

Soil and colluvium did not seem to be an effective sediment source in the Study Area. This can be explained by the correlation with higher soil and colluvium depths with lower slope and IC values (Figure S2) and poor soil cover in the watersheds of the Group A. S impacts on sediment yield are maximized when it occurs at the feet of high cliffs where soil cover is relevant (Figure S2)), and spalls are mixed with organic debris and soil particles to dam channels and trigger debris flows. In the Montiferru area, this combination occurs at the periphery of eroded domes, covered by soils and colluvium. New, postfire soil and colluvium detachment areas may correspond to zones where thicker soil cover is associated with accumulation of spalling fragments (Figure S2). As a result, spalls can compose up to the 36% of the postfire debris flow deposits total volume.

Thermal spalling occurrence is clearly associated with specific land cover, rock type and burn severities (Fig. 5). Spalls concentration in the observed postfire debris flow deposits ranges between 1.3 and 36.6%. This means that these parameters can be effective predictors of postfire debris flow and erosion hazard and should be included in hazard assessment and soil erosion modeling. In this case higher thermal spalling percentages are clearly associated with high and moderate high burn severities, shrubberies and forests and fractured rock types such as tephrite-phonolite lavas in place as lava domes or displaced and now part of the Pliocene Montiferru Volcanic Complex debris avalanche deposits.

As a result, the impact of the wildfire on sediment formation is a two-stage and complex process, starting during the fire and continuing until postfire erosion is active. We suggest that the most effective impact occurs when spalling fragments are transported as debris flows that, in turn, trigger further erosion on soil and colluvium. Therefore, hazard assessments should use burn severity data (Figure S2) along with prefire geological, geomorphological, and land cover maps given their association of thermal spalling (Fig. 5a, b, c). These maps will help identify affected areas and the main processes likely triggered by the fire. Studying prefire processes and sediment distribution helps understand debris availability and potential damming in channels. Rockfall runout modelling is a useful tool to identify areas with higher boulder concentrations (Fig. 7, Figure S3), which is crucial since boulders are highly susceptible to wildfire-induced thermal spalling, contributing to the generation of new debris^{18,19,44}. Since thermal spalling reduces the size of existing boulders less shear stress is needed to mobilize this sediment after the fire. These insights are valuable for civil protection planning and enhancing debris flow modelling. However, further research is necessary to better understand how wildfires cause erosion through thermal spalling, including physics-based modelling to assess how spalled material could mechanistically increase postfire debris flow likelihood. This will include studying factors like thermal conductivity, porosity, moisture retention, mineralogy, and crack density of lithotypes.

This study show the importance of understanding geological, geomorphological and wildfire processes to improve not only debris flow hazard but also soil erosion understanding and modelling. Fast, cheap and effective debris flow hazard assessment can be improved with IC maps, Rockfall modelling, existing Land cover and Geological Maps and Burn severity.

Conclusions

The Montiferru wildfire affected an area of 131 km²was marked by 80% of moderate high to high severity and costed more than 6 million euros. The fire also heavily impacted the geomorphology of the area, reactivating sediment detachment processes. Field surveys suggested that thermal spalling acted as an effective erosive agent, associated with increased rockfall due to weakened surfaces, and increased slope instability. Thermal spalling was particularly effective on tephrite and phonolite lavas, due to their low thermal conductivity and mineral structural changes induced by heating. Rock exposures and large boulders became sediment sources for postfire

debris flows, in addition to burnt soil. In the two years following the wildfire, 33 debris flows occurred, triggered by three rainstorms.

Our investigations highlight the role of synfire geological, geomorphological and prefire landcover in fostering post wildfire widespread soil erosion and postfire debris flow occurrence showing clearly Wildfire and Geology impacts on the investigated phenomena.

Sediment Connectivity Indexes, Rockfall modelling, Land cover and Geological maps should be included in postfire debris flow and erosion assessment to improve hazard prediction and soil erosion modelling. In particular rockfall modelling, land cover, geology and burn severity maps are effective at highlighting synfire erosional and depositional dynamics directly related to thermal spalling.

As a concluding remark future investigation over burnt scars must include not only prefire and postfire investigation but also synfire phenomena.

Methods

This section describes the methods and data used to study the landforms and processes before, during, and after the wildfire. It includes:

- Dating of rainstorms triggering debris flows through field surveys and local reports and news.
- Data Collection and mapping of gravitational processes through field surveysand remote sensing data (aerial photos and satellite images) which were used to map and analyze the landforms. Orthophotos and satellite images helped locate and map the morphologies, with a validation through field surveys.
- Burn Severity Mapping: through Sentinel-2 satellite images, which were created to create a burn severity map using the Normalized Burn Ratio (NBR) index.
- Soil and colluvium thickness Maps: thickness maps were created using field measurements and interpolation techniques.
- Rockfall Simulation throughthe STONE program, which simulated rockfall trajectories using a digital elevation model and other coefficients.
- Thermal Spalling Survey throughfield surveys, which measured spall thickness, eroded percentages, and mapped eroded rock exposures.
- Sediment Connectivity Index which was calculated using GIS tools to estimate surface roughness and drainage characteristics.

These methods provided a comprehensive understanding of the geological and geomorphological changes in the study area due to the wildfire and rainfall.

Triggering rainstorms identification

Field surveys were conducted immediately after the postfire debris flow triggered by rainfall. In addition, the landslides that occurred on 3 November 2021 were also dated by interviewing local civil protection volunteers and reading their written reports⁵¹ as well as local new reports about these landslide phenomena⁵². The phenomena occurring on 30 September 2022 and 21 November 2021 was validated through field surveys only, performed immediately after the rainfall events.

The rainstorms are described through the analysis of the rainfall cumulative data publicly available at ARPAS website for the years 2021 and 2022 from the 20/07/2021 to the 30/11/2022^{53,54}. We used the data collected by the raingauge stations of 'Cuglieri RU', 'Cuglieri C.Ra Tega' and 'Santu Lussurgiu RU'.

The data was merged, and a hydrograph was built for each station looking at the cumulates recorded on the day when postfire debris flows occurred.

Data collection and mapping

New geological and geomorphological data were obtained by recognizing and mapping landforms before, during, and after the fire. This involved field surveys and analyzing remote sensing data. High-resolution orthophotos and satellite images taken after the fire helped map the landforms accurately. The data collected was validated through field surveys. Here is a simplified list of satellite images and aerial photos used to characterize the prefire and post-fire environments:

Aerial photos:

- IGM (Italian Geographical), 1968, Scale: 1:23,000.
- ETFAS, 1977, Scale: 1:10,000.
- AGEA, 2019, Scale: 1:5,000, Resolution: 20 cm.

Satellite images:

- ESA Sentinel-2, May 2022, Resolution: 10 m.
- Pleiades tri-stereo, February 2022, Resolution: 30 cm.

Burn severity mapping method

The perimeter, area, and burn severity of the 2021 Montiferru-Planargia wildfire were determined using Level 2 multispectral ESA Sentinel-2 images with 10 m and 20 m spatial resolution. These images, acquired on 22/07/2021 and 31/07/2021, were processed using the Semi-Automatic Classification Tool in QGIS 3.28⁵⁵. The Burn Severity Map was created by calculating the Normalized Burn Ratio (NBR), which uses near infrared (NIR) and shortwave infrared (SWIR) wavelengths⁴¹. The difference between pre-fire and post-fire NBR values

(dNBR) indicates burn severity, with higher values showing more severe damage and negative values indicating healthy vegetation or regrowth.

Once the dNBR is calculated, it is processed in the GIS environment to create a burn severity map using the classification proposed by the USGS (Table S1)⁴¹.

Map of the thickness

Soil and colluvium measurements were performed on August 2022. The pre-erosional surface was still visible at sites were rill-interrill erosion and earth pyramid erosion occurred. Measurements on eroded thickness were added as an uncertainty to the soil and colluvium maps. The map of thickness was created using Inverse Distance Weighting (IDW) interpolation in QGIS 3.28, based on 632 field measurements taken mainly along roads and trails. These measurements were supplemented with 0 values (rock exposures) from aerial and satellite data. Two maps were produced, showing soil and colluvium thickness, with a distance coefficient of 2 and a resolution of 10×10 pixels.

Rockfall simulation

The rockfall simulation was conducted using the STONE program, which creates maps showing rockfall paths, boulder heights, and maximum velocities based on a Digital Elevation Model (DEM)⁵⁶. The simulation used a 10-meter resolution DEM from www.sardegnageoportale.it. Coefficients for rolling friction, normal, and tangential restitution were assigned based on similar studies, reclassifying lithology and land cover⁵⁷. The lithology (Table S2, Figure S4) was assessed using new stratigraphic units and reclassified according to uniaxial compressive strength values⁵⁸.

In the study area, marls and limestones are not prone to rockfall, so they are classified as Moderately Hard Rock due to their mechanical similarity to some Miocene pyroclastic deposits. Pliocene Debris Avalanche and Debris Flow Deposits are considered as soils in the modelling phase, despite containing large blocks of lavas and pyroclastic deposits, and are classified as Very Soft Rock. Land cover was reclassified into six classes based on similar land use (Table S3, Figure S5). Using ArcMAP 10.8.2, terrain classes were created by combining different data (Table S4). Coefficient values from literature were used to assign ranges for each rock class. Rolling friction, normal, and tangential restitution coefficients vary with land cover. Forested areas have the lowest rolling friction and highest normal and tangential restitution coefficients, while bare soil has the highest rolling friction and lowest normal and tangential restitution coefficients. The data is repeatedly tested and adjusted through simulations until the trajectories match well with the areas covered by boulders (Figure S2). The final values, shown in Table S4, provide the best simulation results, covering the highest percentage of boulders.

To assign initial values to each class, we collected modeling values from literature for each lithological class. We then adjusted these values to simulate land cover changes. Forests were given the lowest rolling friction coefficients and the highest normal and tangential restitution coefficients, while bare soil areas were given the highest rolling friction coefficients and the lowest normal and tangential restitution coefficients. To validate the simulation results, satellite data from 5/14/2022 was used to map 15,332 boulders (Figure S2) with diameters greater than 0.5 m. The data was considered calibrated when the simulated trajectories matched the boulder locations well (Figure S3, Table S4). The validated values were used to create the trajectories map, and each detachment area was reclassified into three classes based on the number of simulated trajectories.

Thermal spalling surveying

A survey was conducted to measure spall thickness, eroded percentages, and map eroded rock exposures and deposits. Photos of rock exposures were taken ensuring they were parallel to the rock to maintain proportions. Eroded percentages were calculated using FIJI (ImageJ2) by dividing the spalled area by the total rock surface area and multiplying by 100. The survey also mapped rock exposures using QGIS 3.34 to determine burn severity. Crack distances were measured to calculate crack density.

The presence of rocky debris derived from thermal spalling had been investigated on photos taken during field surveys. We used the software JMicroVision v1.3.5 to perform a modal analysis through the Point Counting tool. Spalls percentages had been investigated establishing two classes (spalls, other debris), the point counting threshold was set to 1000 points for each investigated deposit. The investigation area was constrained to the photo portion representing the deposit. Grain size estimates are provided for a deposit placed under a rocky cliff eroded by fire. Classes distribution is calculated on a photo of the deposit with point counting function on I-MicroVision version 1.3.5.

Sediment connectivity index calculation

Sediment connectivity index (IC) has been calculated on ArcGis Pro 3.4.3 environment following the procedure proposed by applying D-Infinity algorithms as suggested by 1. The W index we applied is the roughness index proposed by 2 since most of the area has no vegetation cover.

The algorithms used for IC calculation are Slope, Flow Direction, Flow Accumulation and Flow Length available in Spatial Analyst toolbox. Roughness index had been calculated with the Focal Statistics function available in the Image Analyst with mean and standard deviation statistic types.

Hazard parameters selection and investigation

We performed, on a QGIS 3.34 Prizren environment, a statistical analysis of investigated parameters across the burnt watersheds. Parameters were sampled through the Zonal Statistics tool. Watersheds were splitted in two groups based on their geomorphological response to rainfall. The first group comprises all the watersheds which experienced debris flow activity, second one the remaining. We choose to investigate distribution of average sediment connectivity index, average and maximum slope, maximum rockfall intersections, mode of

soil and colluvium depths, areas covered by excavation of afforestation terraces before the fire and observed thermal spalling percentages. These values are in part under investigation during this study while others are well investigated and known for their effectiveness in predicting the investigated hazards. Since the values have different order of magnitudes a z-normalization was performed over selected values with the normalize function available on Microsoft Office Excel.

Data availability

The datasets generated and/or analyzed in this study are available in the Zenodo repository: RAW DATA - The Montiferru-Planargia 2021 wildfire: a type case for quantifying the impact of thermal spalling in debris-flow triggering (https://doi.org/10.5281/zenodo.15235426). Access is temporarily restricted and will be made public ly available upon publication. Those wishing to access the repository should contact the corresponding author.

Received: 4 March 2025; Accepted: 8 August 2025

Published online: 22 August 2025

References

- 1. De Bano, L. F. Water Repellent Soils: A State-of-the-Art. 1-17 (1981).
- Verma, S. & Jayakumar, S. Impact of forest fire on physical, chemical and biological properties of soil: A review. Impact Fire Phys. Chem. Biol. Prop. Soil. Rev. 2, 168–176 (2012).
- 3. Giordano, A. Pedologia Forestale E Conservazione Del Suolovol. 1 (UTET, 2002).
- 4. Alcañiz, M., Outeiro, L., Francos, M. & Úbeda, X. Effects of prescribed fires on soil properties: A review. Sci. Total Environ. 613-614, 944-957 (2018).
- 5. Agbeshie, A. A., Abugre, S., Atta-Darkwa, T. & Awuah, R. A review of the effects of forest fire on soil properties. J. Res. 33, 1419–1441 (2022).
- 6. Imeson, A. C., Verstraten, J. M., Mulligen, E. J. & Sevink, J. The effects of fire and water repellency on infiltration and runoff under mediterrenean type forest. *Eff. Fire Water Repellency Infiltration Runoff Mediterrenean Type For.* **19**, 345–361 (1992).
- 7. Ortíz-Rodríguez, A. J., Muñoz-Robles, C. & Borselli, L. Changes in connectivity and hydrological efficiency following wildland fires in Sierra madre oriental, Mexico. Sci. Total Environ. 655, 112–128 (2019).
- 8. Martini, L. et al. Evaluating the effects of forest cover changes on sediment connectivity in a catchment affected by multiple wildfires. In *Innovative Biosystems Engineering for Sustainable Agriculture, Forestry and Food Production* Vol. 67 (eds Coppola, A., Di Renzo, G. C., Altieri, G., D'Antonio et al.) 13–20 (Springer International Publishing, 2020).
- 9. Wittow, J. The Penguin Dictionary of Physical Geography (Peguin Books, 1984).
- 10. Wohl, E. E. Rivers in the Landscape: Science and Management (John Wiley & Sons, Incorporated, 2014).
- 11. Yin, J. et al. Drought-related wildfire accounts for one-third of the forest wildfires in subtropical China. Agric. Meteorol. 346, 109893 (2024).
- 12. Ohno, I., Harada, K. & Yoshitomi, C. Temperature variation of elastic constants of quartz across the α β transition. *Phys. Chem. Min.* **33**, 1–9 (2006).
- 13. Johnson, S. E., Song, W. J., Cook, A. C., Vel, S. S. & Gerbi, C. C. The quartz $\alpha \leftrightarrow \beta$ phase transition: does it drive damage and reaction in continental crust? *Earth Planet. Sci. Lett.* **553**, 116622 (2021).
- 14. Xu, H., Veblen, D. R. & Zhang, Y. Structural modulation and phase transition in a Na-rich alkali feldspar. *Am. Mineral.* **80**, 897–906 (1995).
- 15. Padilla, I., López-Delgado, A. & Romero, M. Kinetic study of the transformation of sodalite to nepheline. *J. Am. Ceram. Soc.* 105, 4336–4347 (2022).
- 16. Hasselman, D. P. H. Effect of cracks on thermal conductivity. J. Compos. Mater. 12, 403-407 (1978).
- 17. Shen, Y. L., Abdo, M. G. & Van Rooyen, I. J. Thermal conductivity of crack-containing media: A numerical study. *J. Compos. Mater.* 56, 2495–2508 (2022).
- 18. Dorn, R. I. Boulder weathering and erosion associated with a wildfire, Sierra Ancha mountains, Arizona. *Geomorphology* 55, 155–171 (2003).
- 19. Buckman, S., Morris, R. H. & Bourman, R. P. Fire-induced rock spalling as a mechanism of weathering responsible for flared slope and Inselberg development. *Nat. Commun.* 12, 2150 (2021).
- 20. Larsson, K. Fires in tunnels and their effect on rock a review. Luleå University of Technology, Department of Civil and Environmental Engineering, Research Report, 69 pp. (2006).
- 21. Shtober-Zisu, N. & Wittenberg, L. Long-term effects of wildfire on rock weathering and soil stoniness in the mediterranean landscapes. Sci. Total Environ. 762, 143125 (2021).
- 22. Melzner, S., Shtober-Zisu, N., Katz, O. & Wittenberg, L. Brief communication: Post-wildfire rockfall risk in the Eastern alps. *Nat. Hazards Earth Syst. Sci.* 19, 2879–2885 (2019).
- 23. Sarro, R. et al. Effects of wildfire on rockfall occurrence: A review through actual cases in Spain. Appl. Sci. 11, 2545 (2021).
- Pérez-Rey, I. et al. A brief review of the effect of wildfires on rockfall occurrence. IOP Conf. Ser. Earth Environ. Sci. 1124, 012122 (2023).
- Zhang, P., Nordlund, E., Mainali, G., Saiang, C., Jansson, R. & Adl-Zarrabi, B. Experimental study on thermal spalling of rock blocks exposed to fire. Luleå University of Technology & SP Technical Research Institute of Sweden, Technical Report, 12 pp. (2009).
- 26. Wasantha, P. L. P., Guerrieri, M. & Xu, T. Effects of tunnel fires on the mechanical behaviour of rocks in the vicinity A review. Tunn. Undergr. Space Technol. 108, 103667 (2021).
- 27. Smith, A. G. & Pells, P. J. N. Impact of fire on tunnels in Hawkesbury sandstone. Tunn. Undergr. Space Technol. 23, 65-74 (2008).
- 28. Clauser, C. & Huenges, E. Thermal Conductivity of Rocks and Minerals. in *AGU Reference Shelf* (ed. Ahrens, T. J.) 105–126American Geophysical Union, Washington, D. C., (1995). https://doi.org/10.1029/RF003p0105
- 29. Loddo, S. Studio Sulla Genesi Di Suoli Sulle Vulcaniti Alcaline Del Montiferru, Sardegna centro-occidentale (IT, 2003).
- 30. Loddo, S. & Melis, M. Landforms and Soils Mediterranean mountain environments. in 65–85 (2012). https://doi.org/10.1002/9781119941156.ch4
- $31. \ \ Tedim, F.\ et\ al.\ Defining\ extreme\ wild fire\ events:\ difficulties,\ challenges,\ and\ impacts.\ \textit{Fire}\ 1,9\ (2018).$
- 32. Murtas, F. & Tanchis, U. Complesso forestale Montiferru Planargia. Presidi Forestali Tresnuraghes-Montresta-Pabarile Progetto esecutivo. 2023-2024-2025. 47 (2023).
- 33. Kottek, M., Grieser, J., Beck, C., Rudolf, B. & Rubel, F. World Map of Koppen-geiger climate Classification updated. (2006).

- 34. Dipartimento della protezione civile commissario delegato incendi 2021 ex ocdpc 789/2021 emergenza & regione autonoma della sardegna. PPrimi interventi urgenti di protezione civile in conseguenza dell'eccezionale diffusione degli incendi boschivi che hanno determinato uno straordinario impatto nei territori colpiti della regione sardegna nell'ultima decade del mese di luglio 2021 piano degli interventi urgenti (articolo 6, comma 1 ocdpc 789/2021). https://www.regione.sardegna.it/documenti/1_38_20220512113347. pdf (2022).
- 35. Fibbi, A. Il Vulcanismo Terziario Basico Della Sardegna Nord-Occidentale (Università degli Studi di Pisa, 1970).
- 36. Zerbi, M., Giammetti, F., Gallo, F. & Vernia, L. Mineralogia dei noduli peridotitici Delle Basnaiti analcitiche superiori Del montiferru, Sardegna. Ateneo Parm Acta Nat. 14, 421-463 (1978).
- 37. Pioli, L., Pala, C. & Naitza, S. Unraveling 20 my of history of a volcanic complex: the Montiferru area (Italy). https://meetingorganizer.copernicus.org/EGU22/EGU22-13324.html (2022). https://doi.org/10.5194/egusphere-egu22-13324
- 38. Deriu, M. et al. Caratteri geopetrografici Del Montiferro centrale (Sardegna). Mem. Della Soc. Geol. Ital. XIII, 415-439 (1974).
- 39. Van Vries, W. & Delcamp, A. B. Volcanic Debris Avalanches. in Landslide Hazards, Risks, and Disasters 131–157 (Elsevier, 2015). https://doi.org/10.1016/B978-0-12-396452-6.00005-7
- 40. Loddo, S., Marrone, A. & Vacca, A. Soils of the Plio-Pleistocenic volcanic district of Montiferru (Central Western Sardinia, Italy). In: Zdruli, P., Steduto, P. & Kapur, S. (eds), 7th International Meeting on Soils with Mediterranean Type of Climate (selected papers), CIHEAM, 157–166 (2002).
- 41. Keeley, J. E. Fire intensity, fire severity and burn severity: a brief review and suggested usage. *Int. J. Wildland Fire.* **18**, 116–126 (2009).
- 42. Calsamiglia, A. et al. Spatial patterns of sediment connectivity in terraced lands: anthropogenic controls of catchment sensitivity. Land. Degrad. Dev. 29, 1198–1210 (2018).
- 43. Moody, J. A. & Nyman, P. Variations in Soil Detachment Rates after Wildfire as a Function of Soil Depth, Flow Properties, and Root Properties. (2013).
- 44. Kendrick, K. J., Partin, C. A. & Graham, R. C. Granitic boulder erosion caused by chaparral wildfire: implications for cosmogenic radionuclide dating of bedrock surfaces. *J. Geol.* **124**, 529–539 (2016).
- 45. Zimmermann, A., Schinn, D. S., Francke, T., Elsenbeer, H. & Zimmermann, B. Uncovering patterns of near-surface saturated hydraulic conductivity in an overland flow-controlled landscape. *Geoderma* **195–196**, 1–11 (2013).
- Cannon, S. H., Bigio, E. R. & Mine, E. A process for fire-related debris flow initiation, Cerro Grande fire, New Mexico. Hydrol. Process. 15, 3011–3023 (2001).
- 47. Langhans, C. et al. Post-fire hillslope debris flows: evidence of a distinct erosion process. Geomorphology 295, 55-75 (2017).
- 48. Nyman, P., Sheridan, G. J., Smith, H. G. & Lane, P. N. J. Evidence of debris flow occurrence after wildfire in upland catchments of south-east Australia. *Geomorphology* 125, 383–401 (2011).
- 49. Blackwelder, E. Fire as an agent in rock weathering. J. Geol. 35, 134-140 (1927).
- 50. Robertson, E. C. Thermal Properties of Rocks. 106 (1988).
- 51. ODV La Fenice Cuglieri. Report sugli interventi realizzati. 15. (2021).
- 52. LinkOristano Maltempo, viabilità a rischio. Auto bloccata nel sottopasso a Terralba e tra il fango a Cuglieri. (2021).
- 53. ARPAS. Dati meteorologici Rete Unica Regionale e Rete Primaria ARPAS Anni 2021-2022-2023. (2025).
- 54. Agenzia regionale per la protezione dell'ambiente della Sardegna (Arpas). Dati meteorologici Rete Unica Regionale e Rete Primaria ARPAS Anno (2022).
- Congedo, L., Semi-Automatic, C. & Plugin A python tool for the download and processing of remote sensing images in QGIS. J. Open. Source Softw. 6, 3172 (2021).
- Guzzetti, F., Crosta, G., Detti, R. & Agliardi, F. Stone: a computer program for the three-dimensional simulation of rock-falls. Comput. Geosci. 28, 1079–1093 (2002).
- 57. Gallo, I. G. et al. An integration of UAV-Based photogrammetry and 3D modelling for rockfall hazard assessment: the cárcavos case in 2018 (Spain). *Remote Sens.* 13, 3450 (2021).
- 58. Sarro, R. et al. Geotechnics for rockfall assessment in the volcanic island of gran canaria (canary islands, Spain). *J. Maps.* **16**, 605–613 (2020).
- 59. Columbu, S. et al. Manuale sui materiali lapidei vulcanici della sardegna centrale e dei loro principali impieghi nel costruito (Iskra edizioni, 2006).
- 60. Borselli, L., Cassi, P. & Torri, D. Prolegomena to sediment and flow connectivity in the landscape: A GIS and field numerical assessment. CATENA 75, 268–277 (2008).
- 61. Cavalli, M., Trevisani, S., Comiti, F. & Marchi, L. Geomorphometric assessment of spatial sediment connectivity in small alpine catchments. *Geomorphology* 188, 31–41 (2013).
- 62. Cavalli, M., Tarolli, P., Marchi, L. & Dalla Fontana, G. The effectiveness of airborne lidar data in the recognition of channel-bed morphology. *CATENA* 73, 249–260 (2008).

Acknowledgements

This work is dedicated to the memory of Stefano Loddo, who passed away just before acceptance of this article. We will miss him greatly both as a good friend and as a valued colleague. The authors are grateful to the Civil Protection Volunteers of Cuglieri for their support in validating the timing of post-fire debris flow events.

Author contributions

Costantino Pala: Formal analysis, Investigation, Methodology, Data curation, Validation, Visualization, Writing—original draft, editing; Maria Teresa Melis: Funding acquisition, Project administration, Methodology, Supervision, Writing—original draft, review & editing; Laura Pioli: Funding acquisition, Conceptualization, Investigation, review & editing; Roberto Sarro: Conceptualization, Data curation, review; Stefano Loddo: Conceptualization, review, Funding acquisition; Salvatore Cinus: Conceptualization, review, Funding acquisition; Maria Teresa Brunetti: Funding acquisition, Methodology, Data curation, review.

Funding

This research was funded by the Autonomous Region of Sardinia's General Directorate of Civil Protection in collaboration with the Department of Chemical and Geological Sciences at the University of Cagliari, Italy, Research Institute for the Hydrogeologic Protection – National Research Council (CNR-IRPI), and PRIN project Wa.Co.Med. to L.P.

Declarations

Competing interests

The authors declare no competing interests.

Additional information

Supplementary Information The online version contains supplementary material available at https://doi.org/1 0.1038/s41598-025-15527-2.

Correspondence and requests for materials should be addressed to C.P.

Reprints and permissions information is available at www.nature.com/reprints.

Publisher's note Springer Nature remains neutral with regard to jurisdictional claims in published maps and institutional affiliations.

Open Access This article is licensed under a Creative Commons Attribution-NonCommercial-NoDerivatives 4.0 International License, which permits any non-commercial use, sharing, distribution and reproduction in any medium or format, as long as you give appropriate credit to the original author(s) and the source, provide a link to the Creative Commons licence, and indicate if you modified the licensed material. You do not have permission under this licence to share adapted material derived from this article or parts of it. The images or other third party material in this article are included in the article's Creative Commons licence, unless indicated otherwise in a credit line to the material. If material is not included in the article's Creative Commons licence and your intended use is not permitted by statutory regulation or exceeds the permitted use, you will need to obtain permission directly from the copyright holder. To view a copy of this licence, visit https://creativecommons.org/licenses/by-nc-nd/4.0/.

© The Author(s) 2025